Eng. Sci., 2022, **20**, 236–243

Engineered Science

DOI: https://dx.doi.org/10.30919/es8d683

Using Periodic Trapezoidal Silver Strips and Silicon Dioxide Slab for Polarization-Independent Narrowband Absorber

Chen Fu and Bo Wang*

Abstract

This paper proposes a perfect electromagnetic absorber composed of a trapezoidal silver metal-dielectric array and a double-layer base layer. Based on the finite element method, the absorber achieves an absorption efficiency in the near-infrared band of 99.91% under transverse-electric (TE) polarization, and 93.40% under transverse-magnetic (TM) polarization. And the accuracy of this calculation result is verified by the finite difference time domain method. By analyzing the distribution of electric field intensity under other parameters, the mechanism of the structure parameters to affect the absorption efficiency is studied. Finally, the manufacturing tolerance of each structural parameter is calculated when the absorption efficiency is above 90%. Trapezoidal perfect narrow-band absorber can be applied in optical sensor and optical detection.

Keywords: Narrowband absorber; Trapezoidal metal-dielectric array; The finite element method.
Received: 11 October 2021; Revised: 19 March 2022; Accepted: 27 March 2022.
Article type: Research article.

1. Introduction

Gratings are widely used in many fields due to their special periodic structure.[1-3] With its unique characteristics of beam splitting, polarization, dispersion, absorption, and phase matching, gratings occupy an important position in optical communications,[4,5] wavelength division multiplexing,[6-9] photoelectric sensors,[10-14] liquid crystal displays,[15-17] and optical signal acquisition and processing.[18-20] The absorber can achieve single-band and multi-band absorption with different structural designs. And the use of different materials can get broad-band and narrowband absorbers.[21-23] *Feng et. al.* designed a wide-angle dual-band infrared perfect absorber based on simple asymmetric T-shaped plasmonic array. The dual-band absorber realizes two distinct absorption peaks at the wavelength 4.61 μm and 6.53 μm. The nature of the absorption is due to the localized surface plasmon polariton (LSPP) mode excited in the cavities. Thus, the two absorption peaks can be tuned independently by changing the cavity length of each cavity.[24] *Wu et al.* presented a polarization independent, wide-angle spectrum selective absorber exhibiting perfect absorption at the infrared wavelength. It contains two pairs of stacked metal-dielectric grating structures. Rigorous coupled-wave analysis (RCWA) and the simulated annealing (SA) algorithm are employed to obtain the optimized structure dimensions of the absorber. Polarization independent near-unity absorption is achieved at the wavelength of 1635 nm.[25] *Lin et al.* investigated the feature of enhanced absorption for polarization-independent broad-band absorbers in the visible regime. The absorbers are three-layered structures consisting of a three-layered structure consisting of a top layer of tungsten (W) grating, a middle layer of polysilicon (p-Si) slab, and a bottom layer of tungsten substrate. Enhanced absorption (A > 80%) occurs over a wide range of wavelength (200 nm) for both polarizations.[26]

This paper presents a narrowband trapezoidal dielectric array absorber using two materials of silver and silicon dioxide in the near-infrared wave, using finite element method[27,28] and finite difference time domain method[29-31] to calculate and analyze. Table 1 lists the comparison between the absorber in this paper and the references. Absorption peaks of 99.91% is simultaneously achieved around the wavelength of 1558 nm for transverse-electric (TE) polarization, and 93.40% is achieved around the wavelength of 1539 nm for transverse-magnetic (TM) polarization. The underlying physics of such perfect absorption effects is also illustrated by investigating the field distribution and power loss density in these absorbers. At last, the relationship between the absorption spectrum and the geometric parameters of the structures is studied. Narrow-band absorber can transform these signals into visual signals by changing the current or conductivity and the optical properties to realize the application of optical sensor and optical detection.

School of Physics and Optoelectronic Engineering, Guangdong University of Technology, Guangzhou 510006, China.
**Email*: wangb_wsx@yeah.net (B. Wang)

Table 1. The comparison between the absorber in this paper and the references.

Grating	Absorption band	Grating structure	Absorption peak	
			TE polarization	TM polarization
Reported Ref. [24]	Dual-band narrowband	T-shaped plasmonic array	—	99.8% at 4610 nm and 99.9% at 6530 nm
Reported Ref. [25]	Single-band narrowband	Tri-layer structure	99.74% at 1635 nm	98.7% at 1635 nm
Reported Ref. [26]	Single-band broadband	Tungsten grating walls	99.9% at 600 nm	99.6% at 609 nm
This paper	Single-band narrowband	Trapezoidal silver metal-dielectric array	99.91% at 1558 nm	93.40% at 1539 nm

2. Structure of polarization-independent narrowband absorber

The illustration of the suggested one-dimensional (1D) absorption structure as well as the propagation configurations of the incident electromagnetic wave are presented in Fig. 1. As depicted in Fig. 1, the trapezoidal grating ridges are periodically arranged on the double-layer dielectric plane with a period d. The upper base of the trapezoidal grating ridge is a, the lower base is b, and the thickness of each grating ridge is h_1. The duty cycle f_1 = a/d and f_2 = b/d. Two-layer metallic ground plane consists of a silicon dioxide layer with a thickness of h_s and a silver layer with a thickness of h_a. Silver is chosen as the metallic components, and the frequency-dependent complex dielectric constants are taken from Ref.[32] The refractive index and dispersion curves of the material used in the grating are shown in Fig. 2. The simulation of the absorber in the near-infrared band is realized by the finite element method. In the finite element method of dielectric periodic structures, the boundary condition is used to truncate the open-domain boundary, and the finite element scheme suitable for the scattering problem of dielectric gratings with arbitrary gate shape is directly established, the method is simple and the algorithm program is universal to any structure. Maxwell's equations in frequency domain are solved by finite element method. The electromagnetic wave propagates along the x-y plane, and the electric field is polarized along the z direction. At the same time, it is assumed that the analog domain is a complete vacuum, so the Maxwell equation in the frequency domain can be simplified to:[33]

$$\nabla \cdot (\mu_r^{-1} \nabla E_z) - k_0^2 \varepsilon_r E_z = 0 \quad (1)$$

Among them, E_z is the electric field, the relative permeability in vacuum, and the dielectric constant is $\mu_r=\varepsilon_r=1$, and k_0 is the wave number. A finite simulation domain and a set of boundary conditions are needed to solve the above equation by the finite element method. A finite simulation domain is a simulation domain with an open boundary, that is, the boundary of the computational domain allows electromagnetic waves to pass through without reflection. The exterior is transparent to all radiation, so some boundary conditions are applied along the exterior to truncate the domain to a reasonable approximation of the free space. It is also desirable to truncate the domain as small as possible, since controlling the size of the model can help reduce computational costs.

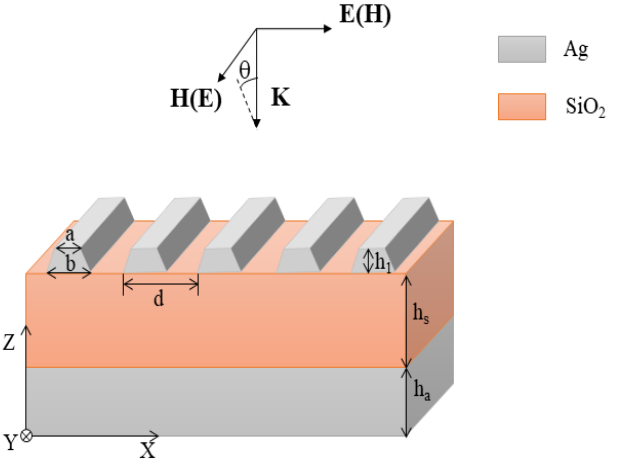

Fig. 1 Schematic of the one-dimensional absorber based on trapezoidal grating ridge consisted of Ag and SiO_2.The optimized dimensions are d=640 nm, f_1=a/d=0.23, f_2=b/d=0.27, h_1=45 nm, h_s=240 nm, h_a=200 nm, respectively.

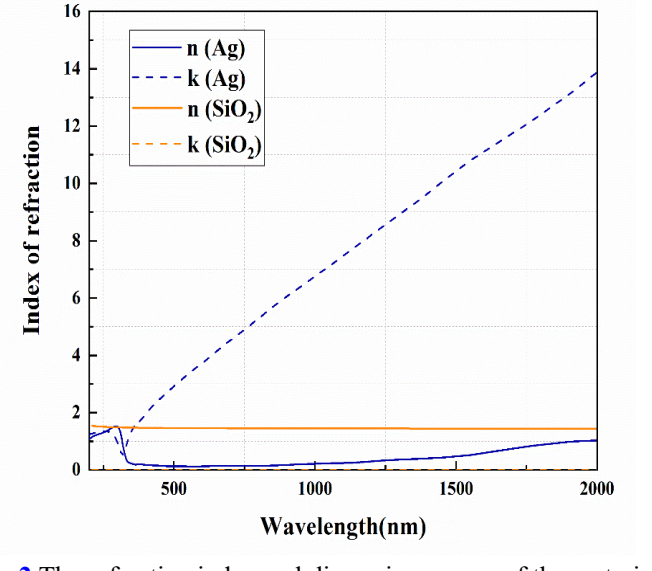

Fig. 2 The refractive index and dispersion curves of the material used in the grating.

The grating structure with trapezoidal grating ridge is modeled and calculated using the wave optics module in COMSOL software. A data analysis is carried out to set a

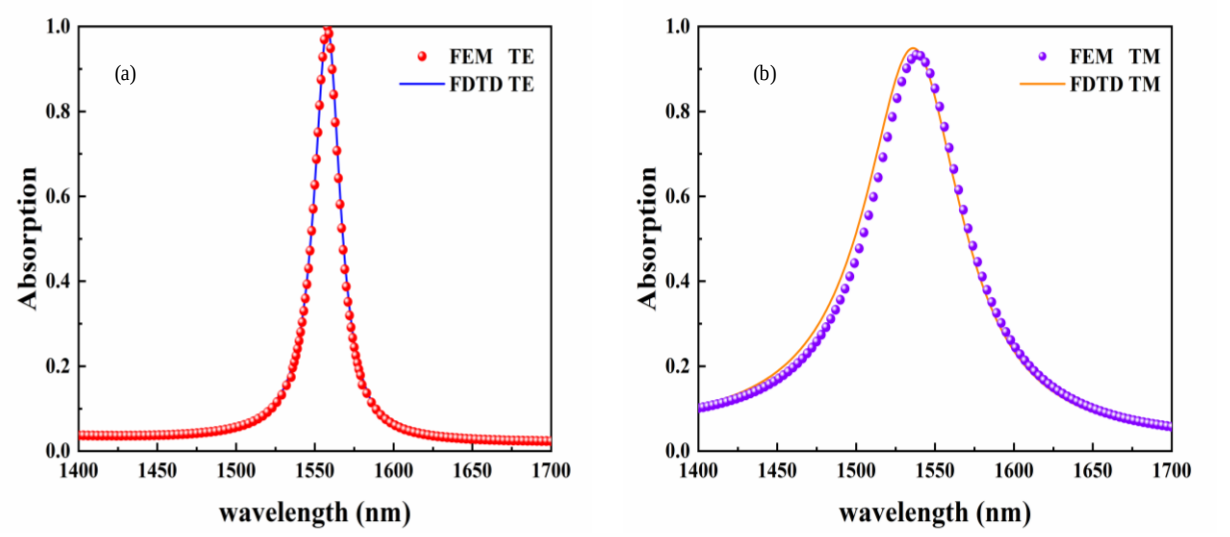

Fig. 3 The absorption spectrum of the near-infrared band calculated by the finite element method and the finite difference time domain method at normal incidence (a) under TE polarization and (b) under TM polarization.

suitable range for the structural parameters of the grating. In the calculation, its structural parameters are: d=640 nm, f_1=a/d=0.23, f_2=b/d=0.27, h_1=45 nm, h_s=240 nm, h_a=200 nm. From the absorption spectrum in Fig. 3, it can be seen that $\eta^{TM}_{\lambda=1539nm} = 93.40\%$, $\eta^{TE}_{\lambda=1558nm} = 99.91\%$. In order to verify the accuracy of the data, the finite difference time domain method is used for verification. By the finite difference time domain method, $\eta^{TM}_{\lambda=1539nm} = 94.39\%$, $\eta^{TE}_{\lambda=1558nm} = 99.89\%$. The results calculated by the two methods are almost completely consistent. By using the wave optics module in COMSOL software, Fig. 4 shows the normalized electromagnetic field distribution at the absorption

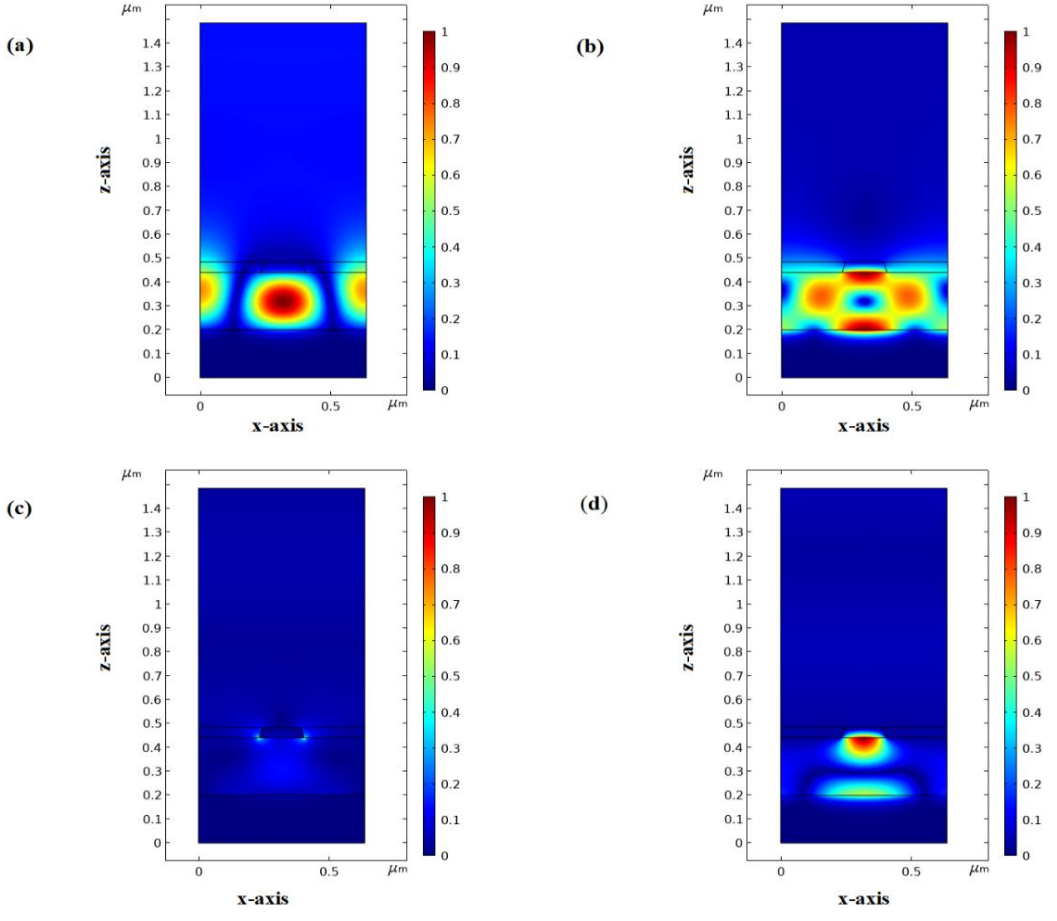

Fig. 4 The normalized electromagnetic field distributions at the resonant wavelength of 1558 nm (TE polarization) and 1539 nm (TM polarization): (a) Electric field and (b) Magnetic field for the TE polarization, (c) Electric field and (d) Magnetic field for the TM polarization.

peak under TE and TM polarization.[34] From Fig. 4(a), it can be seen that the electric field intensity reaches the peak in the center of the silicon dioxide (SiO_2) layer, which is named as Region A. while the magnetic field intensity distribution map of Fig. 4(b) shows a completely opposite intensity distribution. The magnetic field intensity under TE polarization reaches a valley value at the center of the SiO_2 layer and the junction of the two periods of the SiO_2 layer, and the two small areas above and below the center of the SiO_2 layer reach a peak value. Since the absorption depth under TM polarization is not as large as that under-TE polarization, the electromagnetic field distribution under TM polarization in Figs. 4(c) and (d) is not as obvious under TE polarization. However, it can be seen that the electric field intensity reaches the peak value at the two bottom corners of the trapezoidal grating ridge which is named as Region B, and the magnetic field intensity reaches the peak value at the bottom of the trapezoidal grating ridge. In addition to the influence of the transmittance of the base layer and reflection, the absorption of the absorber also accounts for a part of the loss in the metal layer. Fig. 5 analyzes the loss in the metal layer under the two polarizations. The loss under TE polarization is mainly concentrated on the bottom layer of the grating ridge and the upper surface of the silver layer substrate, and the loss of TM polarization is partly concentrated on the very thin layer at the bottom of the grating ridge. The loss of the absorber in the metal layer is greater under TE polarization than under TM polarization.

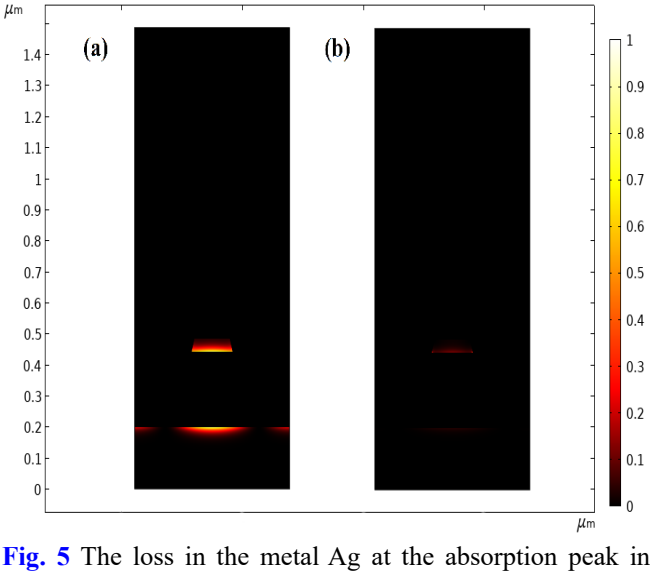

Fig. 5 The loss in the metal Ag at the absorption peak in the contrast of the two polarizations under normal incidence.

3. Analysis and discussions

The tolerance of each structural parameter is continued to be analyzed using COMSOL software based on the finite element method.[35-38] Fig. 6 analyzes the absorption characteristics of an angle change at absorption peaks. The polarized wave with a wavelength of 1558 nm under TE polarization is incident from the air layer into the grating, and the absorber exhibits extremely sensitive angle characteristics. The angle range where the absorption efficiency is higher than 90% is -2° to 2°. Under TM polarization, the absorber exhibits its large-angle insensitivity. Within the angular bandwidth of 152°in [-76°, 76°], the absorption efficiency is higher than 90%. It can also be seen from the calculation results that the absorption efficiency is symmetric about the axis of vertical incidence.

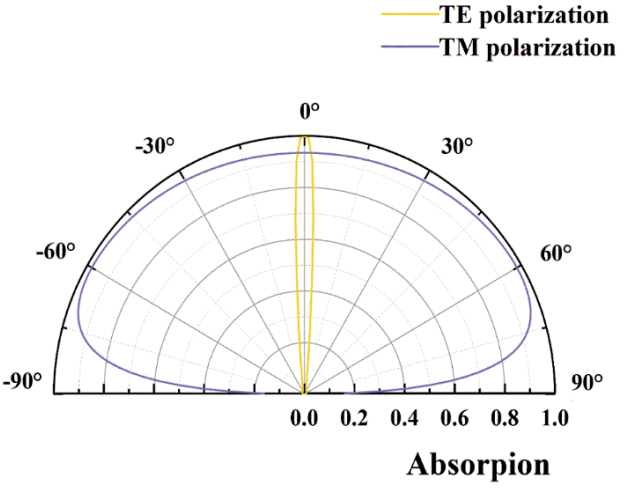

Fig. 6 Polar plot of the absorption of polarization independent 1D perfect absorber as a function of incident angle at the peak wavelength under TE- and TM-wave incidence.

The influence of the duty cycle f_1 and f_2 on the absorption peak is shown in Fig. 7. Under TE polarization, the changing trends of the duty cycles f_1 and f_2 on the absorption peak are roughly the same. When the duty cycle f_1 or f_2 increases, the absorption peak will shift to the left. In Fig. 7(a), take $f_1 = 0.1$ as an example to do a lateral analysis. As the wavelength increases. The diffraction energy of the diffraction wave is increased to enter the inner part of the grating, and the higher absorption efficiency is obtained. When the wavelength increases beyond the diffraction threshold, the diffraction wave energy cannot enter the grating, and the absorption efficiency is close to 0. The electric field intensity diagram shows that when the TE-polarized light diffracted into the grating, the energy concentrates at the SiO_2 layer below the Ag grating ridge, and the f_1 increases, that is, the upper bottom of the grating ridge increases, the blocking of TE-polarized light increases accordingly, which reduces the absorption efficiency under TE polarization. From the electric field intensity diagram of $f_1 = 0.4$ in Fig. 7(b), it can be seen that the energy concentration region moves upward under TM polarization, which explains the reduced absorption efficiency. When η^{TE} is higher than 90%, the satisfied range is $f_1 \in [0.20, 0.29]$ and $\lambda \in [1556\ nm, 1560\ nm]$; $f_2 \in [0.22, 0.29]$ and $\lambda \in [1558\ nm, 1560\ nm]$. In Fig. 7(c), the electric field of TE polarization at $f_2 = 0.1$ and $f_2 = 0.9$ are analyzed, respectively, showing the blocking of energy by the structural parameter a of the grating ridge. Fig. 7(d) shows that the electric field intensity distribution at $f_2 = 0.5$, $\lambda = 1539$ nm is compared with that in Fig. 4(c). the electric field intensity in region B decreases with the increase of f_2. When f_1 is in the range of 0.20-0.27, and λ

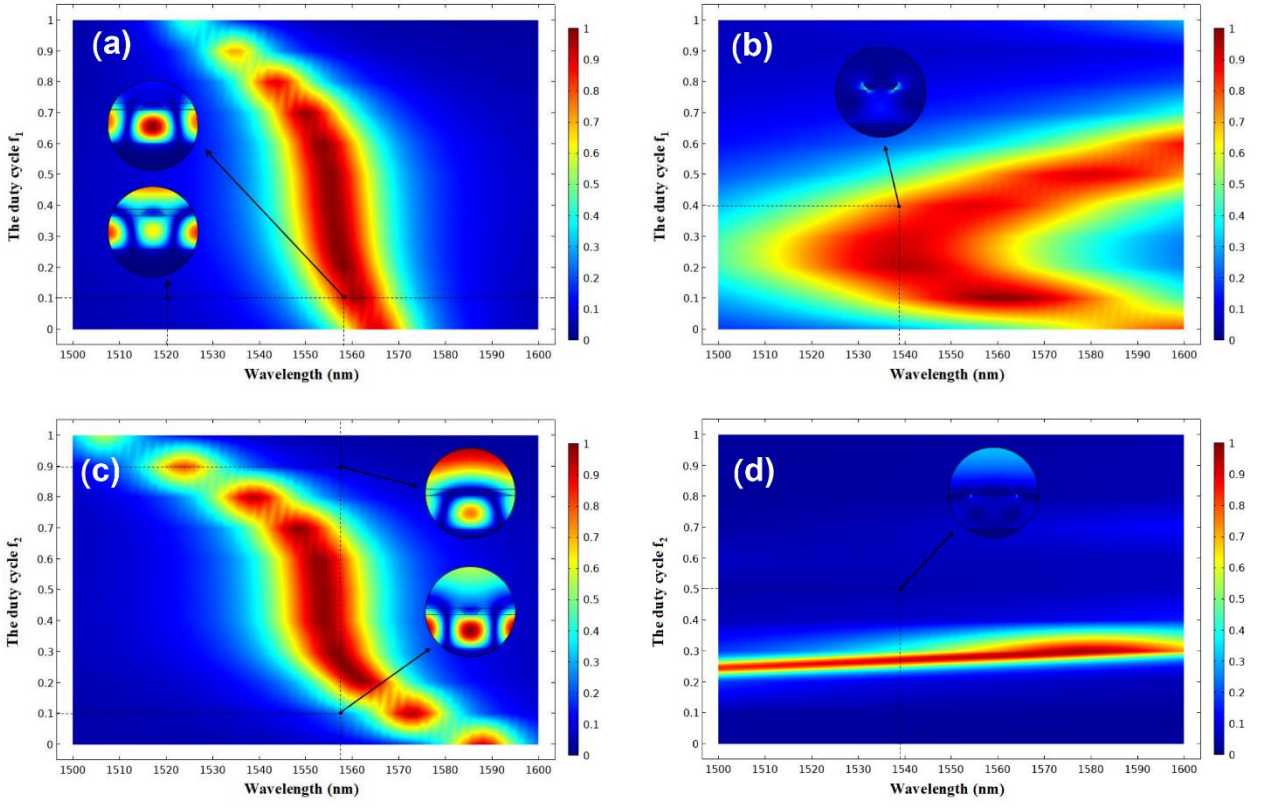

Fig. 7 Absorption as a function of duty cycle: (a) f_1 in TE wave and (b) TM wave, (c) f_2 in TE wave and (d) TM wave from 0 to 1.

is in the range of 1534-1542 nm, η^{TM} is higher than 90%. When f_2 increases, the absorption peak under TM polarization slowly moves to the right. The wavelength λ is in the range of 1532-1544 nm at $f_2 = 0.27$, and the absorption peak is higher than 90%. When TM-polarized light is diffracted into the grating, only the two bottom corners of the grating ridge capture the energy. This explains why Figs. 7(b) and (d) have a smaller tolerance range.

Fig. 8 depicts the influence of h_s on the absorption spectrum. When the thickness of the SiO_2 layer changes, the TE polarization spectrum of the absorber is distributed intermittently; the TM polarization spectrum is striped. Because the energy of TE-polarized light mainly concentrates on the SiO_2 layer whose thickness is h_s, the change of h_s has a great influence on the absorption efficiency of TE-polarized light. As can be seen from Fig. 8(a), the tolerance range at λ = 1558 nm shows a point-like distribution. However, the absorption efficiency under TM polarization is not badly affected by h_s, but confined to its energy capture region, and h_s has a slightly smaller tolerance range. When h_s = 240 nm, the bands with absorption efficiency higher than 90% are [1556 nm, 1560 nm] under TE polarization and [1532 nm, 1544 nm] under TM polarization.

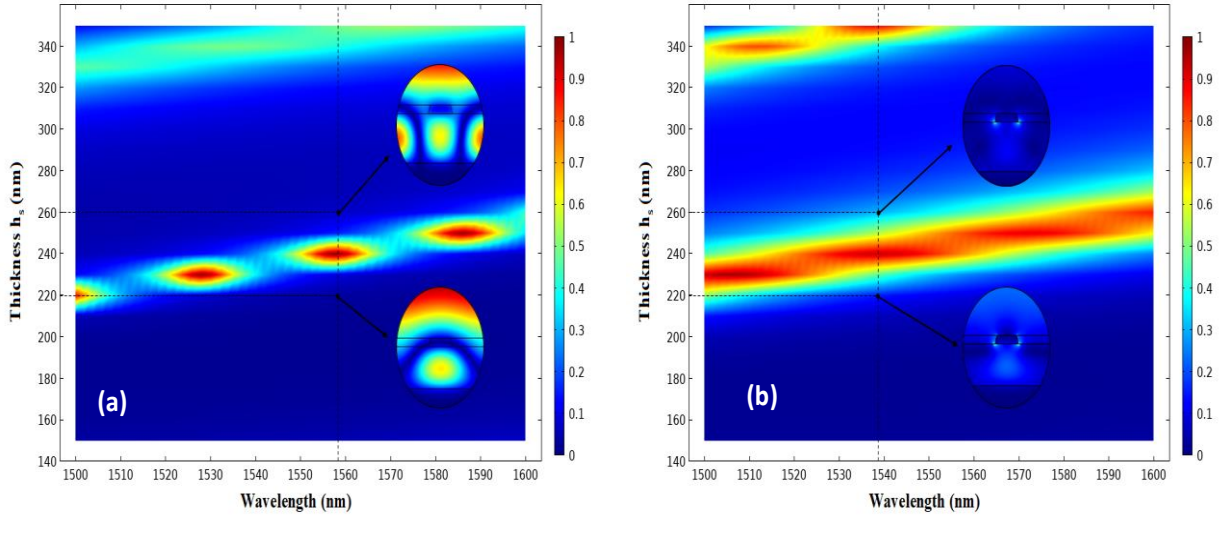

Fig. 8 The influences of silicon dioxide layer thickness h_s on the absorption performances for the (a) TE and (b) TM polarization.

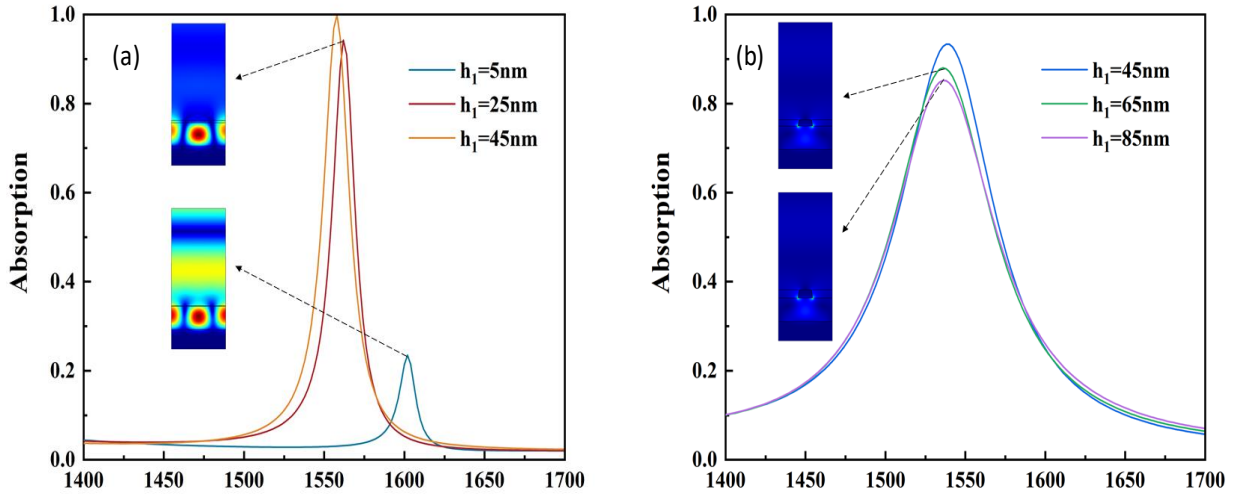

Fig. 9 The influence of different grating ridge thickness h_1 on the absorption peak of the trapezoidal grating ridge absorber for the (a) TE and (b) TM polarization.

In order to find out the influence of the thickness h_1 of the grating ridge on the absorption peak, Fig. 9 describes the change of the absorption spectrum under different h_1. When the step length is 20 nm, h_1 increases, the absorption peak under TE polarization shifts to the right, but the absorption peak under TM does not move much, and the absorption efficiency decreases. By analyzing the electric field intensity distribution at the absorption peak of the absorption curve, it is found that the electric field intensity under TE polarization is more affected by h_1 than that under-TM polarization at the same step length, the main reason is the energy absorption region. When η^{TE} of the absorption peak (λ = 1558 nm) is higher than 90%, the manufacturing tolerance of h_1 is [29 nm, 60 nm]. Under TM polarization, the manufacturing tolerance of h_1 is [32 nm, 54 nm] when λ = 1539 nm.

The correlation between period d and absorption spectrum is investigated. It is observed from Fig. 10 that the manufacturing tolerance of d is larger under TM polarization than under TE polarization in the absorption peak band (1550-1560 nm). As the period increases, the wavelength of the absorption peak also increases, and there is a positive correlation between the two. The manufacturing tolerance of the period d is [638 nm, 642 nm] of TE wave and [632 nm, 651 nm] of TM wave. Similar to the effect mechanism of hs, the absorption efficiency is affected by the energy absorption region of TE polarized light, so the change trend is similar to Fig. 8(a). Under TM polarization, when the absorption efficiency reaches the maximum, a small amount of energy is accumulated in Region A besides Region B. Finally, in order to clearly show the manufacturing tolerances of the absorber, the tolerance ranges of each structural parameter at the absorption peaks under the two polarizations are listed in Table 2.

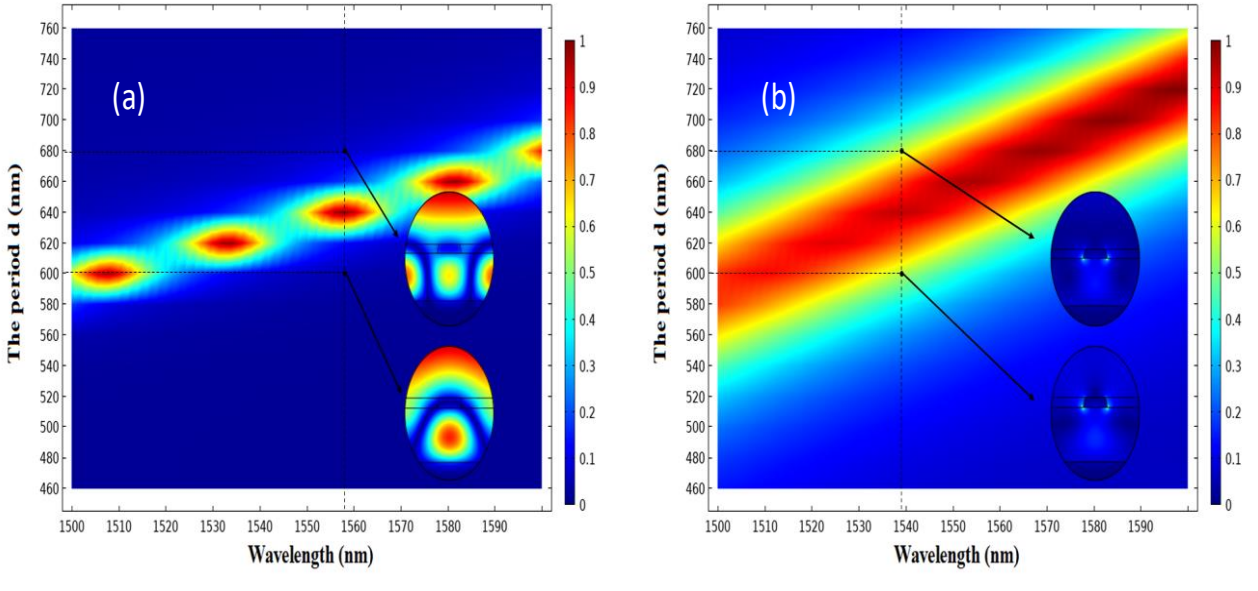

Fig. 10 The influences of the period d of the absorber on the absorption performances for the (a) TE and (b) TM polarization.

Table 2. The manufacturing tolerance of absorber geometrical parameters at the absorption peak with absorption higher than 90%.

Polarizations	Absorption ranges	Fabrication tolerances				
		h1 (nm)	hs (nm)	f1	f2	d (nm)
TE	η>90%	29~60	239~241	0.11~0.50	0.22~0.35	638~642
TM	η0>90%	32~54	238~241	0.14~0.32	0.27	632~651

4. Conclusions

In conclusion, polarization independent 1D perfect absorber based on trapezoidal grating ridge have proposed. This absorber has absorption peaks at the wavelength 1558 nm under TE polarization with the absorption achieve 99.91% at normal incidence. Under TM polarization, the absorption efficiency of 93.40% is achieved at the absorption peak with a wavelength of 1539 nm. It is found that the absorber shows narrow-angle (angle bandwidth is 4°) absorption characteristics under TE polarization and wide-angle (angle bandwidth is 152°) absorption characteristics under TM polarization. The normalized electromagnetic field pattern distribution and the loss generated in the metal layer are explored, which clearly shows the electromagnetic intensity distribution in the absorber. It is found that the structure parameters affect the absorption efficiency by affecting the energy absorption region of the grating. The absorption efficiency under TE polarization is greatly affected by the structure parameters of region A, while the absorption efficiency under TM polarization is greatly affected by region B. Finally, the manufacturing tolerance of each grating structure parameter is calculated. Trapezoidal perfect absorbers have great advantages in optical sensor, optical detection and other fields.

Acknowledgements

This work is supported by the Science and Technology Program of Guangzhou (202002030284, 202007010001).

Conflict of interest

The authors declare no conflict of interest.

Supporting information

Not applicable.

References

[1] S. Zhang, Y. Yin, Z. Lv, D. Gao and X. Wang, 5-Channel Polymer/Silica Hybrid Arrayed Waveguide Grating, *Polymers*, 2020, **12**, 629, doi: 10.3390/polym12030629.

[2] S. Song, F. Liu, L. Qi, Z. Zhang, H. Wang and Y. Zhou, A MoS_2-based broadband and multiband metamaterial absorber in the visible band, *Modern Physics Letters B*, 2020, **34**, 2050397, doi: 10.1142/S0217984920503972.

[3] I. S. Amiri, A. N. Z. Rashed, H. M. A. Kader, A. A. Al-Awamry, I. A. Abd El-Aziz, P. Yupapin and G. Palai, Optical communication transmission systems improvement based on chromatic and polarization mode dispersion compensation simulation management, *Optik*, 2020, **207**, 163853, doi: 10.1016/j.ijleo.2019.163853.

[4] H. Zhang, P. Li, H. Li, J. Song, S. Nakamura and S. P. DenBaars, High polarization and fast modulation speed of dual wavelengths electroluminescence from semipolar (20-21) micro light-emitting diodes with indium tin oxide surface grating, *Applied Physics Letters*, 2020, **117**, 181105, doi: 10.1063/5.0022412.

[5] S. K. Patel, V. Sorathiya, Z. Sbeah, S. Lavadiya, T. K. Nguyen and V. Dhasarathan, Graphene-based tunable infrared multi band absorber, *Optics Communications*, 2020, **474**, 126109, doi: 10.1016/j.optcom.2020.126109.

[6] Y. Liu, Z. Li, D. Li, Y. Yao, J. Du, Z. He and K. Xu, *IEEE Photonics Journal*, 2020, **12**, 4900308, doi: 10.1109/JPHOT.2020.3001595.

[7] L. V. Bartkiv, Y. V. Bobitski and H. Poisel, Optical demultiplexer using a holographic concave grating for POF-WDM systems, *Optica Applicata*, 2005, **35**, 59-66.

[8] D. Mu, H. Qiu, J. Jiang, X. Wang, Z. Fu, Y. Wang, X. Jiang, H. Yu and J. Yang, *IEEE Photonics Journal*, 2019, **11**, 6600708, doi: 10.1109/JPHOT.2019.2897359.

[9] X. Hu, H. Si and H. Shen, Spectral characteristics and space division multiplexing scheme of long period fiber grating pair, *Optik*, 2021, **227**, 166117, doi: 10.1016/j.ijleo.2020.166117.

[10] M. Aslinezhad, High sensitivity refractive index and temperature sensor based on semiconductor metamaterial perfect absorber in the terahertz band, *Optics Communications*, 2020, **463**, 125411, doi: 10.1016/j.optcom.2020.125411.

[11] S. Tan, F. Yan, W. Wang, H. Zhou and Y. Hou, Ultrasensitive sensing with three-dimensional terahertz metamaterial absorber, *Journal of Optics*, 2018, **20**, 055101, doi: 10.1088/2040-8986/aab66e.

[12] J. Bai, S. Zhang, F. Fan, S. Wang, X. Sun, Y. Miao and S. Chang, Tunable broadband THz absorber using vanadium dioxide metamaterials, *Optics Communications*, 2019, **452**, 292-295, doi: 10.1016/j.optcom.2019.07.057.

[13] G. Lan, Z. Jin, J. Nong, P. Luo, C. Guo, Z. Sang, L. Dong and W. Wei, Narrowband perfect absorber based on dielectric-metal metasurface for surface-enhanced infrared sensing, *Applied Sciences*, 2020, **10**, 2295, doi: 10.3390/app10072295.

[14] S. Kang, Z. Qian, V. Rajaram, S. D. Calisgan, A. Alu and M. Rinaldi, Ultra-narrowband metamaterial absorbers for high spectral resolution infrared spectroscopy, *Advanced Optical Materials*, 2019, **7**, 1801236, doi: 10.1002/adom.201801236.

[15] K. C. Heo, J. Yi, J. H. Kwon and J. S. Gwag, High contrast reflective liquid crystal display using a thermochromic reflector, *Journal of Optics*, 2015, **17**, 025401, doi: 10.1088/2040-

8978/17/2/025401.
[16] S. Yin, D. Xiao, J. Liu, K. Li, H. He, S. Jiang, D. Luo, X. Sun, W. Ji and Y. Liu, Reconfigurable chiral metasurface absorbers based on liquid crystals, *IEEE Photonics Journal*, 2018, **10**, 4600909, doi: 10.1109/JPHOT.2018.2878775.
[17] Y.- L. Liao and Y. Zhao, Ultrabroadband absorber using a deep metallic grating with narrow slits, *Optics Communications*, 2015, **334**, 328-331, doi: 10.1016/j.optcom.2014.08.023.
[18] F. Chen, Wide-angle infrared plasmonic perfect absorber based on graphene-silica grating, *Optica Applicata*, 2021, **51**, 87-95, doi: 10.37190/oa210107.
[19] P. Wu, Y. Wang, Z. Yi, Z. Huang, Z. Xu and P. Jiang, A near-infrared multi-band perfect absorber based on 1D gold grating Fabry-Perot structure, *IEEE Access*, 2020, **8**, 72742-72748, doi: 10.1109/ACCESS.2020.2983394.
[20] Y. Yu, Z. Yu and X. Sun, Nonmetallic broadband visible-light absorbers with polarization and incident angle insensitivity, *CLEO: Applications and Technology.* Optica Publishing Group, 2021, doi: 10.1364/CLEO_AT.2021.JTu3A.179.
[21] J. Wu, A polarization insensitive dual-band tunable graphene absorber at the THz frequency, *Physics Letters A*, 2020, **384**, 126890, doi: 10.1016/j.physleta.2020.126890.
[22] F. Liu and L. Qi, A simple two-layer broadband metamaterial absorber for solar cells, *Modern Physics Letters B*, 2021, **35**, 2150291, doi: 10.1142/S0217984921502912.
[23] Y. Cheng, J. Liu, F. Chen, H. Luo and X. Li, Optically switchable broadband metasurface absorber based on square ring shaped photoconductive silicon for terahertz waves, *Physics Letters A*, 2021, **402**, 127345, doi: 10.1016/j.physleta.2021.127345.
[24] R. Feng, W. Ding, L. Liu, L. Chen, J. Qiu and G. Chen, Dual-band infrared perfect absorber based on asymmetric T-shaped plasmonic array, *Optics express*, 2014, **22**, A335- A343, doi: 10.1364/OE.22.00A335.
[25] J. Wu, C. Zhou, J. Yu, H. Cao, S. Li and W. Jia, Polarization-Independent absorber based on a cascaded metal–dielectric grating structure, *IEEE Photonics Technology Letters*, 2014, **26**, 949-952, doi: 10.1109/LPT.2014.2311045.
[26] C.-H. Lin, R.-L. Chern and H.-Y. Lin, Polarization-independent broad-band nearly perfect absorbers in the visible regime, *Optics express*, 2011, **19**, 415-424, doi: 10.1364/OE.19.000415.
[27] C. Cen, Z. Yi, G. Zhang, Y. Zhang, C. Liang, X. Chen, Y. Tang, X. Ye, Y. Yi, J. Wang and J. Hua, Theoretical design of a triple-band perfect metamaterial absorber in the THz frequency range, *Results in Physics*, 2019, **14**, 102463, doi: 10.1016/j.rinp.2019.102463.
[28] Y. Jiang and J. Ma, High-order finite element methods for time-fractional partial differential equations, *Journal of Computational and Applied Mathematics*, 2011, **235**, 3285-3290, doi: 10.1016/j.cam.2011.01.011.
[29] H. Lu, X. Liu, L. Wang, Y. Gong and D. Mao, Ultrafast all-optical switching in nanoplasmonic waveguide with Kerr nonlinear resonator, *Optics express*, 2011, **19**, 2910-2915, doi: 10.1364/OE.19.002910.
[30] X. Wang, J. Zhu, H. Tong, X. Yang, X. Wu, Z. Pang, H. Yang and Y. Qi, A theoretical study of a plasmonic sensor comprising a gold nano-disk array on gold film with a SiO_2 spacer, *Chinese Physics B*, 2019, **28**, 044201, doi: 10.1088/1674-1056/28/4/044201.
[31] B. Zhang, Y. Zhao, Q. Hao, B. Kiraly, I.-C. Khoo, S. Chen and T. Huang, Polarization-independent dual-band infrared perfect absorber based on a metal-dielectric-metal elliptical nanodisk array, *Optics express*, 2011, **19**, 15221-15228, doi: 10.1364/OE.19.015221.
[32] P. B. Johnson and R. W. Christy, Optical constants of the noble metals, *Physical review B*, 1972, **6**, 4370, doi: 10.1103/PhysRevB.6.4370.
[33] W. R. Frei and H. T. Johnson, Finite-element analysis of disorder effects in photonic crystals, *Physical Review B*, 2004, **70**, 165116, doi: 10.1103/PhysRevB.70.165116.
[34] J. Wu, C. Zhou, H. Cao and A. Hu, Polarization-dependent and-independent spectrum selective absorption based on a metallic grating structure, *Optics Communications*, 2013, **309**, 57-63, doi: 10.1016/j.optcom.2013.07.012.
[35] Y. Zhou, Z. Shen, X. Huang, J. Wu, Y. Li, S. Huang and H. Yang, Ultra-wideband water-based metamaterial absorber with temperature insensitivity, *Physics Letters A*, 2019, **383**, 2739-2743, doi: 10.1016/j.physleta.2019.05.050.
[36] D. Yan and J. Li, Tuning control of dual-band terahertz perfect absorber based on graphene single layer, *Laser Physics*, 2019, **29**, 046203, doi: 10.1088/1555-6611/ab05bd.
[37] M. A. Baqir, P. K. Choudhury and M. N. Akhtar, ZrN fractal-graphene-based metamaterial absorber in the visible and near-IR regimes, *Optik*, 2021, **237**, 166769, doi: 10.1016/j.ijleo.2021.166769.
[38] C. Cen, Y. Zhang, C. Liang, X. Chen, Z. Yi, T. Duan, Y. Tang, X. Ye, Y. Yi and S. Xiao, Numerical investigation of a tunable metamaterial perfect absorber consisting of two-intersecting graphene nanoring arrays, *Physics Letters A*, 2019, **383**, 3030-3035, doi: 10.1016/j.physleta.2019.06.028.

Author information

Chen Fu *is currently a master's student of the School of Physics and Optoelectronic Engineering at Guangdong University of Technology. Her research interests include beam splitters and absorbers.*

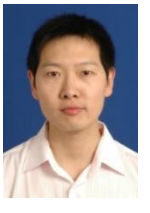

Bo Wang *is a professor of the School of Physics and Optoelectronic Engineering at Guangdong University of Technology. His major research interests include diffraction optics and micro-/nano-optics.*